Soft X-ray Magnetic Circular Dichroism in Paramagnetic Systems: Element-Specific Magnetization of Two Heptanuclear Cr^{III} M^{II}_6 High-Spin Molecules

M.-A. Arrio,[†] A. Scuiller,[‡] Ph. Sainctavit,[†,§] Ch. Cartier dit Moulin,[‡,§] T. Mallah,[‡,||] and M. Verdaguer*[,‡]

Contribution from the Laboratoire de Minéralogie-Cristallographie, CNRS UMR 7590, UPMC/UDD/IPGP, 4 place Jussieu, 75252 Paris Cedex 5, France, Laboratoire de Chimie Inorganique et Matériaux Moléculaires, Unité associée au CNRS No. 7071, Université Paris VI, 4 place Jussieu, 75252 Paris Cedex 5, France, and Laboratoire pour l'Utilisation du Rayonnement Electromagnétique, UMR CNRS 130-CEA-MEN, Université Paris-Sud, BP 34, 91898 Orsay Cedex, France

Received October 5, 1998

Abstract: The local Ni^{II} and Mn^{II} magnetization was measured in the two paramagnetic high-spin molecules $[Cr\{(CN)Ni(tetren)\}_6](ClO_4)_9$ (intramolecular ferromagnetic coupling) and $[Cr\{(CN)Mn(TrispicMeen)\}_6](ClO_4)_9 \cdot 3THF$ (intramolecular antiferromagnetic coupling) by X-ray magnetic circular dichroism (XMCD). The absorption and dichroic spectra were calculated in the ligand field multiplet model to determine the crystal field parameters and the local orientation of the magnetic moments. Local magnetization curves were obtained at the Ni^{II} and Mn^{II} $L_{2,3}$ edges for the two molecules. The behavior of the XMCD signals were followed either by varying the magnetic field at $T = 20$ K or by varying the temperature at $H = 6$ T. The magnetization vs H or T was compared to spin Hamiltonian calculations including spin−spin exchange and Zeeman effect. The local magnetizations for both Ni^{II} and Mn^{II} ions are not proportional to the macroscopic magnetization. The unique potentiality of XMCD applied to the characterization of exchange-coupled elemental spins in paramagnetic compounds is discussed.

Introduction

X-ray magnetic circular dichroism (XMCD) is a recent technique that joins the local selectivity of X-ray absorption spectroscopy to magnetic measurements. XMCD measures the difference in absorption between right and left circularly polarized X-rays. It is expected to give information in complex magnetic systems about the magnetic moment carried by some orbital level of the absorber atom involved in the transitions and the relative orientation of the magnetic moments for the selected elements and orbital levels.[1−3] C. T. Chen and co-workers were the first to use XMCD to deduce local magnetic moments in polymetallic systems.[1] The technique has mostly been used by physicists on metallic compounds.[2] Few applications exist in chemical[3−5] and biochemical systems.[6] Moreover, until recently, XMCD experiments have been only performed on ferromagnetic or ferrimagnetic systems for which a three-dimensional magnetic order exists below a critical temperature T_C. The first experiments on transition metals in paramagnetic compounds were recently performed by Cramer and co-workers in metalloproteins.[5,6] The work presented here is one of the first XMCD experiments performed on paramagnetic compounds[7] and the first in bimetallic polynuclear complexes where the molecular spin states are complex combinations of exchange-coupled local elemental spins.

We chose two examples of high-spin molecules recently synthesized in a bottom-up approach of nanosystems.[8,9] Molecular complexes with spin ground states up to $^{33}/_2$ have been obtained.[8−10] A bimetallic W/Mn system with a $^{39}/_2$ ground state has been recently claimed.[10c] These systems present uniform spin and size and can behave as single-molecule magnets. They can display magnetic anisotropy, long relaxation time, and magnetic quantum tunneling below a blocking temperature.[11,12]

[†] Laboratorie de Minéralogie-Cristallographie.
[‡] Laboratoire de Chimie Inorganique et Matériaux Moléculaires.
[§] Laboratoire pour l'Utilisation du Rayonnement Electromagnétique.
[||] Present address: Laboratoire de Chimie Inorganique, URA 420 CNRS, Bâtiment 420, Université Paris-Sud, 91405 Orsay Cedex, France.

(1) Rudolf, P.; Sette, F.; Tjeng, L. H.; Meigs, G.; Chen, C. T. *J. Magn. Magn. Mater.* **1992**, *109*, 109−112.
(2) Ebert, H.; Schütz, G. *Spin-Orbit Influenced Spectroscopies of Magnetic Solids*; *Lecture notes in Physics*; Springer-Verlag: Berlin, 1996.
(3) Dujardin, E.; Ferlay, S.; Phan, X.; Desplanches, C.; Cartier dit Moulin, Ch.; Sainctavit, Ph.; Baudelet, F.; Dartyge, E.; Veillet, P.; Verdaguer, M. *J. Am. Chem. Soc.* **1998**, *120*, 11347−11352.
(4) Arrio, M. A.; Sainctavit, Ph.; Cartier dit Moulin, Ch.; Brouder, Ch.; de Groot, F. M. F.; Mallah, T.; Verdaguer, M. *J. Phys. Chem.* **1996**, *100*, 4679−4684.
(5) Peng, G.; van Elp, J.; Jang, H.; Que, L., Jr.; Armstrong, W. H.; Cramer, S. P. *J. Am. Chem. Soc.* **1995**, *117*, 2515−2519.
(6) (a) Christiansen, J.; Peng, G.; Young, A. T.; LaCroix, L. B.; Solomon, E. I.; Cramer, S. P. *Inorg. Chim. Act.* **1996**, *243*, 229−232. (b) C. Y. Ralston, Chen, J.; Peng, G.; George, S. J.; van Elp, J.; Cramer, S. P. *Physica B* **1995**, 203−209. (c) van Elp, J.; Peng, G.; Zhou, Z. H.; Mukund, S.; Adams, M. W. W. *Phys. Rev. B.* **1996**, *53*, 2523−2527. (d) George, S. J.; van Elp, J.; Chen, J.; Peng, G.; Mitra-Kirtley, S.; Mullins, O. C.; Cramer, S. P. *Proceedings of the International Conference on Synchrotron Radiation in Biosciences*; Oxford University Press: New York, 1994; pp 313−332.
(7) Schillé, J.-Ph.; Kappler, J.-P.; Sainctavit, Ph.; Cartier dit Moulin, Ch.; Brouder, Ch.; Krill, G. *Phys. Rev. B* **1993**, *48*, 9491−9496.
(8) Mallah, T.; Auberger, C.; Verdaguer, M.; Veillet, P. *J. Chem. Soc. Chem. Commun.* **1995**, *1*, 61−62.
(9) Scuiller, A.; Mallah, T.; Verdaguer, M.; Nivorozhin, A.; Tholence, J.-L.; Veillet, P. *New J. Chem.* **1996**, *20*, 1−3.
(10) (a) Powell, A. K.; Heath, S. L.; Gatteschi, D.; Pardi, L.; Sessoli, R.; Spina, G.; Del Giallo, F.; Pieralli, F. *J. Am. Chem. Soc.* **1995**, *117*, 2491−2502. (b) Scuiller, A. Ph.D. Thesis, Université Pierre et Marie Curie, Paris, 1999. (c) Hashimoto, H.; Zhenng, M., private communication.

10.1021/ja983521j CCC: $18.00
Published on Web 06/25/1999

For the present experiments, one complex is $[Cr\{(CN)Ni(tetren)\}_6](ClO_4)_9$ (tetren = tetraethylenepentamine), noted $Cr^{III}Ni^{II}_6$, with a spin ground-state $S = {}^{15}/_2$ built through a short-range ferromagnetic interaction between the central Cr^{III} ($(t_{2g})^3$) ion and the six Ni^{II} ($(e_g)^2$) ions.[8] The second complex is $[Cr\{(CN)Mn(TrispicMeen)\}_6](ClO_4)_9 \cdot 3THF$ (TrispicMeen = *N*,*N*,*N*′-(tris(2-pyridylmethyl)-*N*′-methylethan)1,2-diamine), noted $Cr^{III}Mn^{II}_6$, with a spin ground-state $S = {}^{27}/_2$ built through an antiferromagnetic interaction between the central Cr^{III} ($(t_{2g})^3$) ion and the six Mn^{II} ($(t_{2g})^5$) ions.[9] Both molecules possess a large spin ground state. Their magnetization at saturation can be reached in reasonable magnetic fields (≤ 7 T) at low temperature which ensures detectable XMCD signals. Another reason for our choice is that the two molecular fragments $Cr^{III}(CN-Ni^{II}-N)_6$ and $Cr^{III}(CN-Mn^{II}-N)_6$ can be considered as building blocks of the three-dimensional Prussian blue analogues, $Cs^I[Ni^{II}Cr^{III}(CN)_6] \cdot 2H_2O$ and $Cs^I[Mn^{II}Cr^{III}(CN)_6]$, the XMCD of which was already measured.[3,4,13]

The edges chosen for XMCD experiments are the transition metal $L_{2,3}$ edges (Ni^{II}, Mn^{II}, and Cr^{III}) corresponding to $2p^63d^n \rightarrow 2p^53d^{n+1}$ transitions. The $L_{2,3}$ edges provide local information about the 3d magnetic orbitals involved in the exchange interaction. The purpose of this paper is to explore the conditions under which XMCD spectroscopy can be used to follow the magnetic properties of each element in paramagnetic polynuclear complexes.

Experimental Section and Theoretical Background

I. Sample Preparation. The preparation and the macroscopic magnetic properties of $Cr^{III}Ni^{II}_6$ and $Cr^{III}Mn^{II}_6$ were already reported.[8,9,10] The coupling constants J between the chromium(III) ion and the nearest neighbors are $+16.8$ cm^{-1} for $Cr^{III}Ni^{II}_6$ and -8 cm^{-1} for $Cr^{III}Mn^{II}_6$.[8-10] The $Ni^{II}-Ni^{II}$ and $Mn^{II}-Mn^{II}$ (next nearest neighbor interactions) are less than -0.5 cm^{-1}.[10b]

II. XMCD Data Collection and Analysis. The experiments were performed on the soft X-ray storage ring Super-ACO at LURE (Orsay, France). The Ni $L_{2,3}$ edges were recorded on the SU22 beamline, where the white beam is monochromatized by a two beryl crystal monochromator, described elsewhere.[14] The Mn^{II} and Cr^{III} $L_{2,3}$ edges were recorded on the SU23 beamline where the monochromator is a plane grating.[15] The circular polarization rate (τ) is 37% at Ni L_3 edge (853 eV)[4] and 70% at Mn and Cr L_3 edges.[15] The spectra were recorded by measuring the photocurrent emitted by the sample. The sample is submitted to a magnetic field from 0 to 7 T delivered by a superconducting magnet[14] and cooled to 20 ± 3 K. During the XMCD experiment, right (or left) circularly polarized X-ray photons are selected. A first spectrum, labeled $\sigma_{\uparrow\uparrow}$, is registered with the magnetic field parallel to the propagation vector of the photons. In the electric dipole approximation, reversing the magnetic field is equivalent to changing the helicity of the beam.[16] A second spectrum, labeled $\sigma_{\uparrow\downarrow}$, is registered with the magnetic field antiparallel to the propagation vector of the photons. The XMCD signal is the difference ($\sigma_{\uparrow\downarrow} - \sigma_{\uparrow\uparrow}$) between the two spectra.

III. Ligand Field Multiplet Calculations. The $L_{2,3}$ edges spectra are calculated by using the ligand field multiplet code developed by Thole[17] in the framework established by Cowan[18] and Butler.[19] This approach takes into account all of the electronic Coulombic repulsions, the spin−orbit coupling on every shell, and treats the geometrical environment of the absorbing atom by a crystal field potential.[20] The spectrum is calculated as the sum of all possible transitions for an electron jumping from the 2p to the 3d level in the electric dipole approximation. No attention is paid to the electric dipole allowed $2p \rightarrow 4s$ transitions that are experimentally and theoretically found to be negligible compared to the $2p \rightarrow 3d$ main channel.[18] As a first approximation, we describe the ground state of the 3d transition metals as a pure $3d^n$ configuration and we calculate the transitions between the $2p^63d^n$ ground-state electronic configuration and the $2p^53d^{n+1}$ excited states. The interelectronic repulsions are introduced through Slater integrals, F^2_{dd} and F^4_{dd} for the ground state and F^2_{dd}, F^4_{dd}, F^2_{pd}, G^1_{pd}, and G^3_{pd} for the excited state. The Slater integrals are calculated by an atomic Hartree−Fock model and are scaled down by a reduction factor κ to reflect the electronic delocalization. The atomic spin−orbit coupling parameters, ζ_{3d} and ζ_{2p}, are calculated from the monoelectronic potential around the free ion.[18] They are slightly adjusted to take into account the modification of the electronic potential by molecular and solid-state effects. The octahedral surrounding of the metal ion is represented by an octahedral crystal field potential whose strength is parametrized by the radial integral $10Dq$.

Results and Discussion

The presentation of the results and the discussion are organized as follows. From the application of sum rules, we determine the ratio of the orbital to the spin magnetic moment contributions M_L/M_S of the Ni^{II} 3d levels in the ferromagnetic $Cr^{III}Ni^{II}_6$ complex (Part I). Then in Part II, the antiferromagnetic interaction between Cr^{III} and Mn^{II} in $Cr^{III}Mn^{II}_6$ is demonstrated. Part III is devoted to the study of the variation of the Ni^{II} and Mn^{II} magnetic moments with the applied magnetic field, whereas Part IV presents the thermal variation of the Ni^{II} 3d magnetic moment.

I. Ni^{2+} XMCD Measured in $Cr^{III}Ni^{II}_6$. The $\sigma_{\uparrow\uparrow}$ and $\sigma_{\uparrow\downarrow}$ absorption spectra and the dichroic signal at Ni^{II} $L_{2,3}$ edges of $Cr^{III}Ni^{II}_6$ are presented in Figure 1. The spectra were recorded at 20 K in an applied magnetic field $H = \pm 6$ T. In the recording conditions the magnetization of the compound represents 60% of the saturation value. The full dichroic signal is the experimental signal normalized to 100% circular polarized light: $\sigma_- - \sigma_+ = 1/\tau(\sigma_{\uparrow\downarrow} - \sigma_{\uparrow\uparrow})$, where the polarization rate τ is determined at each energy of the spectrum.[4] These results can be compared to XMCD measurements at the same edges in the molecule-based magnet, $Cs^INi^{II}[Cr^{III}(CN)_6] \cdot 2H_2O$.[4,13] The $Cr^{III}(CN-Ni^{II}-N)_6$ core of the molecular complex can be seen as an isolated motif of the magnet. There are, nevertheless, important differences in the Ni^{II} environments of the two compounds. In the ferromagnet, each Ni^{II} is bonded to six nitrogens of six cyanide ions, and its local environment is octahedral. In the $Cr^{III}Ni^{II}_6$ high-spin molecule, Ni^{II} is bonded to the nitrogen of one cyanide and to five nitrogens of the tetren ligand. Its local environment is less symmetric than in the associated ferromagnet, since the six nitrogens give a distorted octahedral crystal field. The absorption spectra (see Figure 1)

(11) (a) Sessoli, R.; Gatteschi, D.; Caneschi, A.; Novak, M. A. *Nature* **1993**, 365, 141−143. (b) Gatteschi, D.; Caneschi, A.; Pardi, L.; Sessoli, R. *Science* **1994**, *265*, 1054−1058.

(12) Thomas, L.; Lionti, F.; Ballou, R.; Gatteschi, D.; Sessoli, R.; Barbara, B. *Nature* **1996**, *383*, 145−147.

(13) Arrio, M. A.; Sainctavit, Ph.; Cartier dit Moulin, Ch; Mallah, T.; Verdaguer, M.; Pellegrin, E.; Chen, C. T. *J. Am. Chem. Soc.* **1996**, *118*, 6422−6427.

(14) (a) Sainctavit, Ph.; Lefebvre, D.; Cartier dit Moulin, Ch.; Laffon, C.; Brouder, Ch.; Krill, G.; Schillé, J.-Ph.; Kappler, J.-P.; Goulon J. *J. Appl. Phys.* **1992**, *72*, 1985−1988. (b) Sainctavit, Ph.; Lefebvre, D.; Arrio, M.-A.; Cartier dit Moulin, Ch.; Kappler, J.-P.; Schillé, J.-P.; Krill, G.; Brouder, Ch.; Verdaguer, M. *Jpn. J. Appl. Phys.* **1993**, *32*, 295−298.

(15) Hague, C. F.; Mariot, J. M.; Guo, G. Y.; Hricovini, H.; Krill, G. *Phys. Rev. B* **1995**, *51*, 1370−1373.

(16) Brouder, Ch; Kappler, J.-P. In *Magnetism and Synchrotron Radiation*; Beaurepaire, E., Carrière, B., Kappler, J.-P., Eds.; Les Editions de Physique, 1997; pp 19−32.

(17) Thole, B. T.; van der Laan, G.; Fuggle, J. C.; Sawatzky, G. A.; Karnatak, R. C.; Esteva, J.-M. *Phys. Rev. B* **1985**, *32*, 5107−5118.

(18) Cowan, R. D. *The Theory of Atomic Structure and Spectra*; University of California Press: Berkeley, 1981.

(19) Butler, P. H. *Point Group Symmetry, Applications, Methods and Tables*; Plenum: New York, 1991.

(20) de Groot, F. M. F.; Fuggle, J. C.; Thole, B. T.; Sawatzky, G. A. *Phys. Rev. B* **1990**, *42*, 5459−5468.

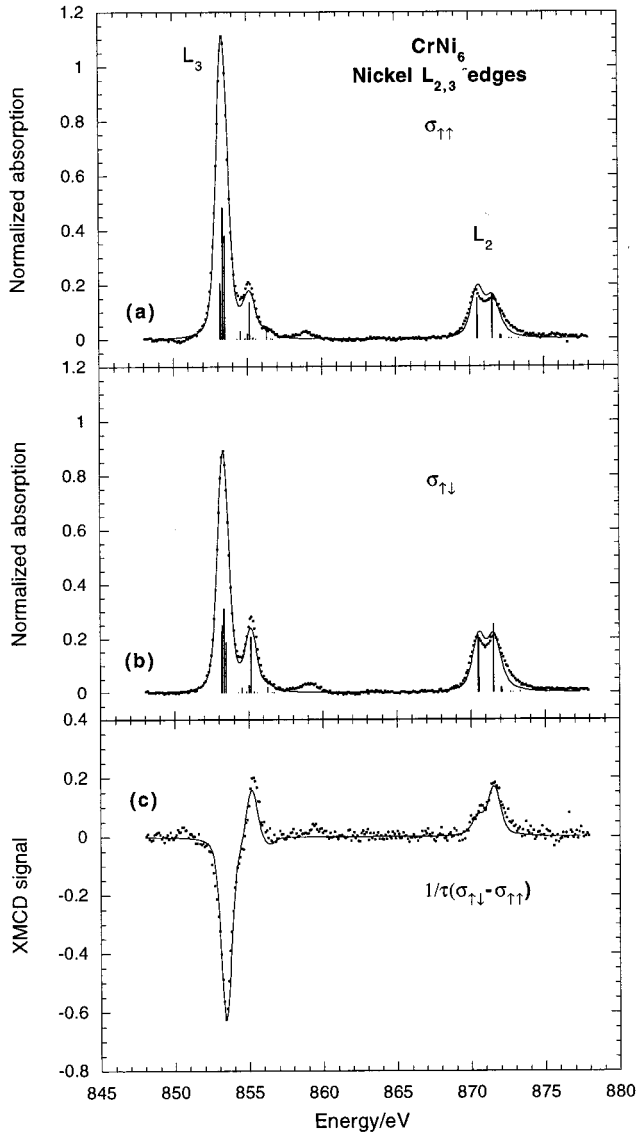

Figure 1. Experimental (dots) and theoretical (line) X-ray absorption at nickel $L_{2,3}$ edges of $Cr^{III}Ni^{II}_6$: (a) $\sigma_{\uparrow\uparrow}$, (b) $\sigma_{\uparrow\downarrow}$, and (c) XMCD signal normalized to 100% circular polarized light. The vertical lines correspond to the individual transition intensities before convolution. The calculation parameters are: $\zeta_{2p} = 11.4$ eV, $\zeta_{3d} = 0.1$ eV, $10Dq = 1.5$ eV.

present two major peaks at the L_3 and the L_2 edge, characteristic of a high-spin Ni^{2+} ion in octahedral symmetry.[21] The small satellite (at 859 eV) between the two edges is the fingerprint of the ligand−metal charge transfer.[4,13,22] The energy positions and intensities of the L_3 peaks of $Cr^{III}Ni^{II}_6$ and $Cs^{I}Ni^{II}[Cr^{III}(CN)_6]\cdot 2H_2O$ spectra are almost the same since Ni^{II} has close local symmetries and crystal field strengths ($10Dq$) in the two compounds. The satellite is 1.5 eV closer to the L_3 edge in the $Cr^{III}Ni^{II}_6$ spectrum than in the $Cs^{I}Ni^{II}[Cr^{III}(CN)_6]\cdot 2H_2O$ spectrum, which demonstrates that the ligand-to-metal charge transfer is larger with the nitrogen of tetren than with the nitrogen of the cyanide.[13]

We performed ligand field multiplet calculations, assuming an octahedral symmetry around Ni^{II} and using a Boltzmann law to take into account the temperature (20 K). The best fit of the absorption spectrum was obtained for $10Dq = 1.5$ eV (vs 1.4 eV in $Cs^{I}Ni^{II}[Cr^{III}(CN)_6]\cdot 2H_2O$), and the Slater integrals reduced to 70% of their atomic value (vs 80% for $Cs^{I}Ni^{II}[Cr^{III}(CN)_6]\cdot 2H_2O$). The result confirms that the covalency of the Ni^{II}−N(tetren) bond is slightly stronger than the covalency of the Ni^{II}−N(C) bond.

The $Cr^{III}Ni^{II}_6$ dichroic signal at the nickel $L_{2,3}$ edges is very similar to the $Cs^{I}Ni^{II}[Cr^{III}(CN)_6]\cdot 2H_2O$ one.[4] The calculations show that the crystal field strength and the covalency mostly act on the intensity of the signal. Thus, even if the calculation parameters are different in the two componds, the dichroic signal is the same.

It is possible to extract the magnetic moment carried by Ni^{II} from the experimental spectra by using the simple relations between the intensities of the dichroic signals of the L_3 and the L_2 edges, provided by the so-called sum rules.[23] Sum rules obtain the spin magnetic moment ($M_S = -2\langle Sz\rangle\mu_B$, μ_B is the Bohr magneton), the orbital magnetic moment ($M_L = -\langle Lz\rangle\mu_B$) and the total magnetic moment ($M = M_S + M_L$) where $\langle Sz\rangle$ ($\langle Lz\rangle$) stands for the Sz (Lz) operator value in the ground state. The sum rules are

$$\langle Lz\rangle = \langle\phi_i|Lz|\phi_i\rangle = -2(10-n)\frac{\int_{L3+L2}(\sigma_- - \sigma_+)\frac{1}{\hbar\omega}\,d(\hbar\omega)}{\int_{L3+L2}\sigma_{iso}\frac{1}{\hbar\omega}\,d(\hbar\omega)}$$

and

$$\langle Sz\rangle = \langle\phi_i|Sz|\phi_i\rangle = -\frac{3(10-n)}{2}\times \frac{\int_{L3}(\sigma_- - \sigma_+)\frac{1}{\hbar\omega}\,d(\hbar\omega) - 2\int_{L2}(\sigma_- - \sigma_+)\frac{1}{\hbar\omega}\,d(\hbar\omega)}{\int_{L3+L2}\sigma_{iso}\frac{1}{\hbar\omega}\,d(\hbar w)} - \frac{7}{2}\langle\phi_i|T_z|\phi_i\rangle$$

$\hbar\omega$ is the incident photon energy and σ_{iso} the isotropic cross section. Tz is the magnetic dipole operator which value is usually considered to be zero in an octahedral environment. We checked this assumption in the present case by a close examination of the ground state determined by the ligand field multiplet calculations.[4,23]

The two sum rules yield M_L/M_S

$$\frac{M_L}{M_S} = \frac{1}{2}\frac{\int_{L3+L2}(\sigma_- - \sigma_+)\frac{1}{\hbar\omega}\,d(\hbar\omega)}{\int_{L3}(\sigma_- - \sigma_+)\frac{1}{\hbar\omega}\,d(\hbar\omega) - 2\int_{L2}(\sigma_- - \sigma_+)\frac{1}{\hbar\omega}\,d(\hbar\omega)} \quad (1)$$

Applying eq 1 to the nickel $L_{2,3}$ edges in $Cr^{III}Ni^{II}_6$ we obtained $M_L/M_S = 0.07$, lower than the ratio found in $Cs^{I}Ni^{II}[Cr^{III}(CN)_6]\cdot 2H_2O$ (0.12).[4] The difference is due to crystal field and charge-transfer effects which appear larger in $Cr^{III}Ni^{II}_6$ than in

(21) van der Laan, G.; Thole, B. T.; Sawatzky, G. A.; Verdaguer, M. *Phys. Rev. B* **1988**, *37*, 6587−6589.

(22) van der Laan, G.; Zaanen, J.; Sawatzky, G. A.; Karnatak, R.; Esteva, J.-M. *Phys. Rev. B* **1986**, *33*, 4253−4263.

(23) (a) Carra, P.; König, H.; Thole, B. T.; Altarelli, M. *Physica B* **1993**, *192*, 182−190. (b) Thole, T.; Carra, P.; Sette, F.; van der Laan, G. *Phys. Rev. Lett.* **1992**, *68*, 1943−1946.(c) Altarelli, M. *Phys. Rev. B* **1993**, *47*, 597−598. (d) Carra, P.; Thole, B. T.; Altarelli, M.; Wang, X. *Phys. Rev. Lett*. **1993**, *70*, 694−697. (e) Altarelli, M.; Sainctavit, Ph. *Magnetism and Synchrotron Radiation*; Beaurepaire, E., Carrière, B., Kappler, J.-P., Eds.; Les Editions de Physique, 1997; pp 65−74.

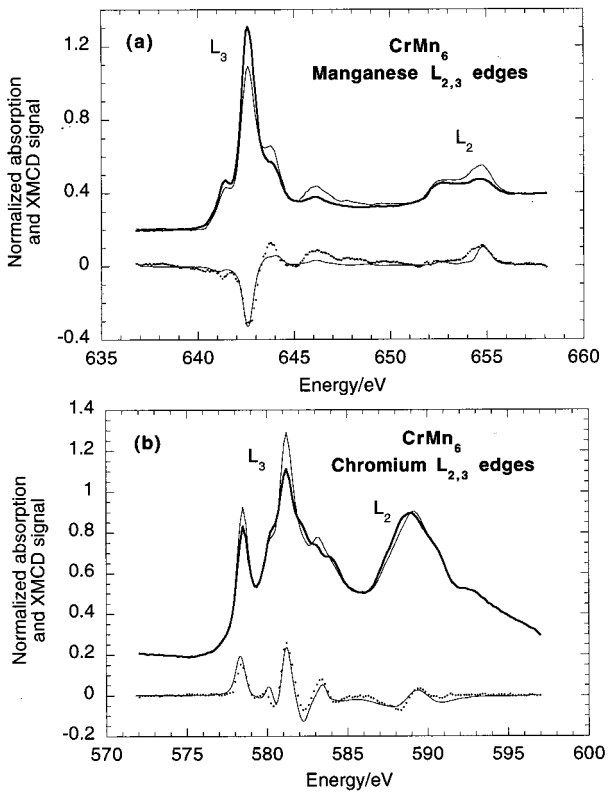

Figure 2. (a) Top, experimental X-ray absorption manganese $L_{2,3}$ edges of $Cr^{III}Mn^{II}_6$: $\sigma_{\uparrow\uparrow}$ (thick line) and $\sigma_{\uparrow\downarrow}$ (thin line). Bottom, experimental (dots) and theoretical (line) XMCD signal normalized to 100% circular polarized light. Calculation parameters: $\zeta_{2p} = 7.0$ eV, $\zeta_{3d} = 0.04$ eV, $10Dq = 0.8$ eV. (b) Top, experimental chromium $L_{2,3}$ edges of $Cr^{III}Mn^{II}_6$: $\sigma_{\uparrow\uparrow}$ (thick line) and $\sigma_{\uparrow\downarrow}$ (thin line). Bottom, experimental (dots) and theoretical (line) XMCD signal normalized to 100% circular polarized light. Calculation parameters: $\zeta_{2p} = 5.67$ eV, $\zeta_{3d} = 0.035$ eV, $10Dq = 3.5$ eV.

$Cs^{I}Ni^{II}[Cr^{III}(CN)_6]\cdot 2H_2O$. M_S is not affected by these parameters and is the same for the two compounds. Thus the quenching of M_L appears more important in $Cr^{III}Ni^{II}_6$.

II. Antiferromagnetic Interaction in $Cr^{III}Mn^{II}_6$. Figure 2 presents the XMCD spectra measured in $Cr^{III}Mn^{II}_6$ at Cr and Mn $L_{2,3}$ edges. The experiments were performed at $H = 4$ T and $T = 20$ K. In these conditions the compound reaches about 65% of the saturation magnetization. For pure metallic elements such as iron, cobalt, or nickel, a negative XMCD signal at the L_3 edge and a positive one at the L_2 edge indicates a local magnetic moment parallel to the exchange magnetic field. In these simple cases, the nature of the exchange interaction between two ions can be deduced from the sign of the XMCD signal.[1,2] When many multiplet states for the final-state configurations are present (as in $2p^5d^4$ and $2p^5d^6$), one observes numerous features in the absorption and in the XMCD spectra. Moreover, for the cyanide C-bond chromium ions, the strong charge transfer yields many structures between the two edges. In such cases, it is not possible to determine by a simple examination of the spectrum the direction of the local magnetic moment respective to the exchange or external magnetic field. To obtain this information, ligand field multiplet calculations are then essential.

The Mn^{II} $L_{2,3}$ absorption spectrum is the fingerprint of a high-spin Mn^{II} ion in octahedral symmetry engaged in weakly covalent bonds. They are very similar to those measured on the three-dimensional molecule-based magnet $Cs^{I}Mn^{II}[Cr^{III}(CN)_6]\cdot 2H_2O$.[13] The absorption and dichroic spectra were calculated with the same parameters used for $Cs^{I}Mn^{II}[Cr^{III}(CN)_6]\cdot 2H_2O$ (O_h symmetry and $10Dq = 0.8$ eV). The theoretical and the experimental XMCD spectra are compared in Figure 2a. The dichroism calculation was performed with an external magnetic field parallel to the Mn^{II} magnetic moment. The main features are well reproduced, which confirms that the Mn^{II} magnetic moment and the magnetic field directions are the same.

The Cr^{III} $L_{2,3}$ absorption spectra are also similar to those measured on $Cs^{I}Mn^{II}[Cr^{III}(CN)_6]\cdot 2H_2O$.[13] The Cr^{III} ion is exactly in the same environment in both compounds, and the same parameters were taken to calculate the edges and the XMCD signal.[13] The calculation is more intricate than that at the Mn^{II} edges because of a strong crystal field effect ($10Dq = 3.5$ eV), a high covalency (the Slater integrals are reduced to 50% of their atomic value), and the large π bonding between the Cr^{III} ion and the cyanide ligand. Taking into account all of these chemical characteristics, the dichroic spectrum at Cr^{III} $L_{2,3}$ edges was calculated with a magnetic field antiparallel to the Cr^{III} magnetic moment, according to the antiferromagnetic coupling between the Mn^{II} and Cr^{III} ions. The computed and experimental XMCD spectra are compared in Figure 2b. The calculation fits well the experimental spectra for the shape as well as for the sign, which shows that the Cr^{III} magnetic moment is indeed in the direction opposite that of the external magnetic field. The XMCD experiments and calculation at the Mn^{II} and at the Cr^{III} $L_{2,3}$ edges confirm the antiferromagnetic coupling between Mn^{II} and Cr^{III} at the local level. The element-specific XMCD measurements compared to the calculations permit the determination a priori of the absolute orientation of the magnetic moment of different metallic absorbers in the magnetic field without the need of preliminary knowledge of the nature of the coupling between them.[3]

The application of the sum rules to determine the ratio M_L/M_S (eq 1) is unfortunately impossible for Cr^{III} and Mn^{II} because the strong overlap between the L_3 and L_2 edges completely prevents the application of the M_S sum rule (see the denominator in eq 1): when ζ_{2p} is not large compared to the Slater integrals (as in the early 3d transition elements), the L_3 and L_2 edges do not adequately separate the $(2p^5)_{j=3/2}3d^{n+1}$ from the $(2p^5)_{j=1/2}3d^{n+1}$ states[24] ($\zeta_{2p} = 5.67$ eV for Cr^{III} vs 11.45 eV for Ni^{II}).

III. Variations of the Ni^{II} and Mn^{II} Local Magnetic Moments with the Magnetic Field in $Cr^{III}Ni^{II}_6$ and $Cr^{III}Mn^{II}_6$. To follow the variation of the local magnetic moments of the metallic ions, we performed XMCD measurements in variable applied magnetic fields. The technique was already used to measure element-specific hysteresis in multilayer compounds.[25] Our goal is to compare (i) experimental and computed magnetization for Ni^{II} and Mn^{II} and (ii) the elemental moments with the molecular ones. In complex systems, when the different molecular spin states are mixtures of local spins, the elemental local magnetic moments given by XMCD experiments do not follow a priori the same behavior as that of the molecular one. We explored up to which point the phenomenon can be measured in the present experimental conditions.

The experiments were performed at the Ni^{II} L_3 edge for $Cr^{III}Ni^{II}_6$ and at the Mn^{II} L_3 edge for $Cr^{III}Mn^{II}_6$ at $T = 20$ K by varying the magnetic field from 1 to 7 T. The Mn^{II} and the Ni^{II} L_3 XMCD signals are both made of two main peaks, one negative, the other positive (Figures 1 and 2a). In the data analysis we checked that the ratio of the area of these two

(24) Teramura, Y.; Tanaka, A.; Jo, T. *J. Phys. Soc. Jpn.* **1996**, *65*, 1053−1055.

(25) Chen, C. T.; Idzerda, Y. U.; Lin, H.-J.; Meigs, G.; Chaban, E. E., Park, J.-H.; Ho, G. H. *Phys. Rev. B* **1993**, *48*, 642−645.

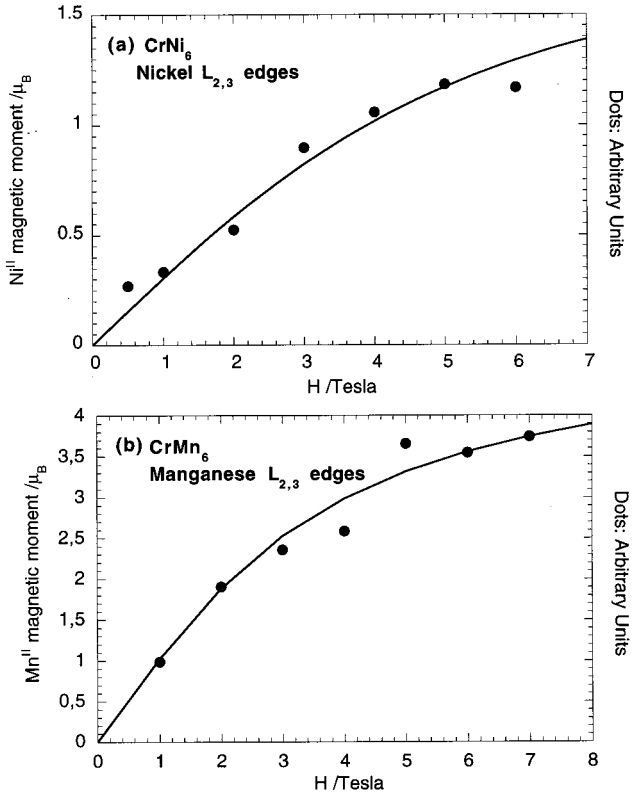

Figure 3. **(a)** Experimental XMCD area at the Ni^{II} L_3 edge vs H (●) compared to the theoretical Ni^{II}-specific magnetization curve of $Cr^{III}Ni^{II}_6$ calculated for $T = 20$ K and $g = 2$ (line). (b) Experimental XMCD area at the Mn^{II} L_3 edge vs H (●) compared to the theoretical Mn^{II}-specific magnetization curve of $Cr^{III}Mn^{II}_6$ calculated for $T = 20$ K and $g = 2$ (line).

peaks stays the same when varying the magnetic field intensity as it is predicted by the calculations. For the two compounds, $Cr^{III}Ni^{II}_6$ and $Cr^{III}Mn^{II}_6$, the areas $\int_{L3} |\sigma_{\downarrow\uparrow} - \sigma_{\uparrow\uparrow}|\, d(\hbar\omega)$ are reported in Figure 3 as a function of the magnetic field (dots in arbitrary units). Since the areas are proportional to the local magnetic moment, the experimental dots have been scaled to be compared to the theoretical magnetization curve, expressed in Bohr magneton per divalent ion (Ni^{II} or Mn^{II}).

At the experimental temperature (20 K), the magnetization vs H curves cannot be fitted by a Brillouin function using a single-spin ground state ($S = {}^{15}/_2$ for $Cr^{III}Ni^{II}_6$ and $S = {}^{27}/_2$ for $Cr^{III}Mn^{II}_6$). The first excited states above the ground state are populated because the recording temperature ($T = 20$ K) is not negligible compared to the coupling constants in the two compounds: $J = +16.8$ cm^{-1} (~24 K) for $Cr^{III}Ni^{II}_6$ and $J = -8$ cm^{-1} (~12 K) for $Cr^{III}Mn^{II}_6$. To obtain the magnetization vs H for the $Cr^{III}Ni^{II}_6$ complex, we calculate the spin states $|(S_{Cr},S_{6Ni})S,m_s\rangle$. The functions are issued from the coupling of the Cr^{III} ion to the six Ni^{II} ions. $\mathbf{S_{Cr}}$ is the Cr^{III} spin operator (S_{Cr} is the associated value of $\mathbf{S^2_{Cr}}$, $S_{Cr} = {}^3/_2$) and $\mathbf{S_{6Ni}}$ the six Ni^{II} spin operator defined by $\mathbf{S_{6Ni}} = \sum_{n=1}^{6}\mathbf{S_{Ni(}}_{\mathbf{n}}\mathbf{_{)}}$ (S_{6Ni} is the associated value of $\mathbf{S^2_{6Ni}}$, $0 \le S_{6Ni} \le 6$). $\mathbf{S}$ is the total spin operator defined by $\mathbf{S} = \mathbf{S_{Cr}} + \mathbf{S_{6Ni}}$. Thus, S is associated with $\mathbf{S^2}$ and m_S is the eigenvalue of $\mathbf{S_z}$. Assuming an external magnetic field H along the z axis ($H = H_z$), the spin Hamiltonian of the system can be written as

$$H = -J\mathbf{S_{Cr}}\mathbf{S_{6Ni}} + g\mu_B\mathbf{S}_z H_z \qquad (2)$$

In eq 2 we assume that $g = g_{Ni} = g_{Cr} = 2$ and that the direct Ni^{II}−Ni^{II} interaction is negligible (it was measured as −0.5 cm^{-1}).[10b] The $|S,m_s\rangle$ functions are eigenfunctions of $\mathbf{S^2}$, $\mathbf{S_z}$, $\mathbf{S^2_{Cr}}$ and $\mathbf{S^2_{6Ni}}$[26] and thus of the Hamiltonian. The energy of a $|(S_{Cr},S_{6Ni})S,m_s\rangle$ state is

$$E(|(S_{Cr},S_{6Ni})S,m_S\rangle) = -\frac{J}{2}[S(S+1) - S_{Cr}(S_{Cr}+1) - S_{6Ni}(S_{6Ni}+1)] + g\mu_B H_z m_S \quad (3)$$

Table 1 gives the energy and the degeneracy of states $(S_{Cr},S_{6Ni})S$ in zero field. The total magnetic moment (M) is calculated using a Boltzmann distribution. Figure 4 compares the theoretical total magnetization curves calculated at $T = 20$ K taking into account either the $S = {}^{15}/_2$ ground state only or all of the spin states: one cannot neglect the contribution of the excited spin states.

Table 1. Energy and Degeneracy of the Spin States $|(S_{Cr},S_{6Ni})S,m_S\rangle$ of the $Cr^{III}Ni^{II}_6$ Molecule in Zero Field: S_{6Ni}, S ($S_{Cr} = {}^3/_2$ for all of the States)[a]

i	S_{6Ni}	S	degeneracy	E_i/J
1	6	${}^{15}/_2$	1 × 16	−9
2	5	${}^{13}/_2$	5 × 14	$-{}^{15}/_2$
3	4	${}^{11}/_2$	15 × 12	−6
4	3	${}^9/_2$	29 × 10	−9/2
5	2	${}^7/_2$	40 × 8	−3
6	6	${}^{13}/_2$	1 × 14	$-{}^3/_2$
7	1	${}^5/_2$	36 × 6	$-{}^3/_2$
8	5	${}^{11}/_2$	5 × 12	−1
9	4	${}^9/_2$	15 × 10	$-{}^1/_2$
10	3	${}^7/_2$	29 × 8	0
11	0	${}^3/_2$	15 × 4	0
12	2	${}^5/_2$	40 × 6	${}^1/_2$
13	1	${}^3/_2$	36 × 4	1
14	1	${}^1/_2$	36 × 2	${}^5/_2$
15	2	${}^3/_2$	40 × 4	3
16	3	${}^5/_2$	29 × 6	${}^7/_2$
17	4	${}^7/_2$	15 × 8	4
18	5	${}^9/_2$	5 × 10	${}^9/_2$
19	2	${}^1/_2$	40 × 2	${}^9/_2$
20	6	${}^{11}/_2$	1 × 12	5
21	3	${}^3/_2$	29 × 4	6
22	4	${}^5/_2$	15 × 6	${}^{15}/_2$
23	5	${}^7/_2$	5 × 8	9
24	6	${}^9/_2$	1 × 10	${}^{21}/_2$

[a] The degeneracy is the number of states with the same (S_{6Ni}, S) multiplied by the spin degeneracy ($2S + 1$).

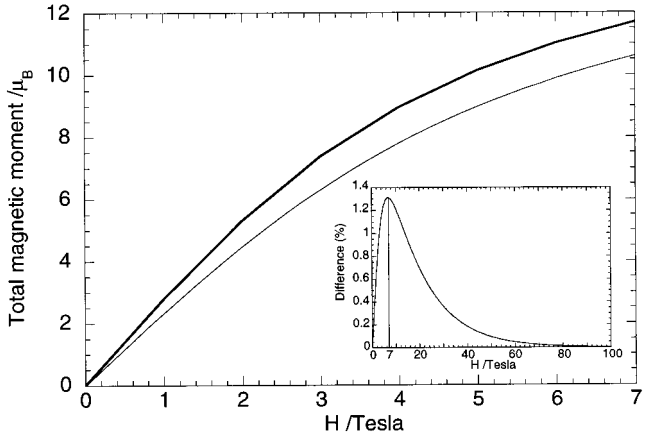

Figure 4. Total magnetization vs H of $Cr^{III}Ni^{II}_6$ calculated at $T = 20$ K taking into account: the $S = {}^{15}/_2$ ground state only (thick line); all of the spin states (thin line). Insert: difference between the normalized theoretical magnetization vs H of the Ni^{II} element and of the $Cr^{III}Ni^{II}_6$ molecule, calculated at $T = 20$ K.

(26) Weissbluth, M. *Atoms and Molecules*; Academic Press INC: San Diego, 1978.

The XMCD experiments measure the local moment carried by the absorber atom. To compare the computed XMCD curve to the experimental results, we have to calculate the elemental moment by decoupling the functions $|(S_{Cr},S_{6Ni})S,m_S\rangle$ which are not eigenfunction of $\mathbf{S}_{z_{6Ni}}$. The Ni^{II} magnetic moment (M_{Ni}) at a given temperature is given by the Boltzmann distribution of $-2\langle \mathbf{Sz_{Ni}}\rangle\ \mu_B$ over the spin states, where

$$\langle \mathbf{S}_{z_{Ni}}\rangle = \langle (S_{Cr},S_{6Ni})S,m_S|\mathbf{S}_{z_{Ni}}|(S_{Cr},S_{6Ni})S,m_S\rangle = \frac{1}{6}\langle (S_{Cr},S_{6Ni})S,m_S|\mathbf{S}_{z_{6Ni}}|(S_{Cr},S_{6Ni})S,m_S\rangle = \frac{1}{6}\delta_{S_{6Ni}S'_{6Ni}}\,\delta_{m_{S6Ni}m'_{S6Ni}}\,\delta_{m_{SCr}m'_{SCr}}\sum_{m_{sCr}=-3/2}^{3/2}\sum_{m_{S_{6Ni}}=-S_{6Ni}}^{S_{6Ni}} C(S_{Cr}m_{SCr},S_{6Ni}m_{S6Ni};Sm_S)^2\ m_{S6Ni} \quad (4)$$

$C(S_{Cr}\ m_{SCr},S_{6Ni}\ m_{S6Ni};S\ m_S)$ is the Clebsh−Gordan coefficient corresponding to the coupling of $|S_{Cr},m_{SCr}\rangle$ with $|S_{6Ni},m_{S_{6Ni}}\rangle$. The Ni^{II}-specific magnetization curve vs H_z was calculated at 20 K. The difference between the weighted Ni^{II} magnetization curve (divided by the Ni^{II} saturation moment 2 μ_B) and the weighted molecular magnetization curve (divided by the total saturation moment 15 μ_B) is reported in the insert of Figure 4. For a given temperature, the difference increases with the magnetic field, reaches a maximum and then decreases when the Zeeman splitting becomes large compared to the temperature. The higher the temperature, the larger will be the difference at the maximum. The difference is less than 1.4% in the magnetic field and in the temperature ranges of our XMCD experiments but shows that the theoretical Ni^{II} magnetic moment is close to the molecular one, but not rigorously proportional.

The calculated Ni^{II} local magnetization is compared with the experimental XMCD magnetization in Figure 3a. We performed calculations with different values of the temperature between 10 and 25 K. The best agreement between experiment and calculation is obtained for $T = 20$ K, the sample temperature. The result shows that the variations of the Ni L_3 XMCD signal follow the Ni^{II}-specific magnetization which is for this compound very close to the macroscopic magnetization.

The local magnetization curve was then measured by XMCD at the Mn^{II} L_3 edge in $Cr^{III}Mn^{II}_6$. The magnetization curve obtained by calculating the area of the absolute dichroic signal is shown in Figure 3b. A spin Hamiltonian similar to the one of $Cr^{III}Ni^{II}_6$ was used to calculate the specific Mn^{II} magnetization curve. We neglected the small zero-field splitting.[9] All of the $Cr^{III}Mn^{II}_6$ spin states are included in the calculation. Figure 3b compares the calculation with the experimental magnetization curve. The best fit was again obtained for the sample temperature $T = 20$ K. In the $Cr^{III}Mn^{II}_6$ molecule, the calculation shows, even with an antiferromagnetic coupling, that the Mn^{II} L_3 XMCD signal follows the Mn^{II}-specific magnetization curve. The difference between the Mn^{II} magnetic moment (divided by 5 μ_B, the Mn^{II} saturation moment) and the total magnetic moment (divided by 27 μ_B, the molecular saturation moment) have been calculated and is less than 0.6%.

One should notice that for $Cr^{III}Ni^{II}_6$ the magnetic moment carried by one nickel ion would be proportional to the total magnetic moment at $T = 0$ K, that is when the states with $S \leq {}^{13}/_2$ are not populated, because the $|S = {}^{15}/_2, m_S = -{}^{15}/_2\rangle$ ground state is uniquely built from coupling of the $|S_{Ni} = 6, m_{SNi} = -6\rangle$ wave function of Ni^{II} and the $|S_{Cr} = {}^3/_2, m_{SCr} = -3/2\rangle$ wave function of Cr^{III}. In the case of $Cr^{III}Mn^{II}_6$, the picture is different because the $|S = {}^{27}/_2, m_S = -{}^{27}/_2\rangle$ ground state arise from the combination of four wave functions

$$|S_{Mn} = {}^{30}/_2, m_{SMn} = {}^{30}/_2\rangle|S_{Cr} = {}^3/_2, m_{SCr} = -{}^3/_2\rangle,$$
$$|S_{Mn} = {}^{30}/_2, m_{SMn} = {}^{28}/_2\rangle|S_{Cr} = {}^3/_2, m_{SCr} = -{}^1/_2\rangle,$$
$$|S_{Mn} = {}^{30}/_2, m_{SMn} = {}^{26}/_2\rangle|S_{Cr} = {}^3/_2, m_{SCr} = {}^1/_2\rangle \text{ and}$$
$$|S_{Mn} = {}^{30}/_2, m_{SMn} = {}^{24}/_2\rangle|S_{Cr} = {}^3/_2, m_{SCr} = {}^3/_2\rangle$$

It means that at $T = 0$ K the magnetic moment of Cr^{III} or Mn^{II} can never be exactly proportional to the total magnetic moment of the molecule. The difference between the Cr^{III} magnetic moment (divided by 3 μ_B) and the total magnetic moment (divided by 27 μ_B) can reach 7%. The origin of this behavior for $Cr^{III}Mn^{II}_6$ is to be found in the antiferromagnetic coupling between the ions contrary to the situation in the ferromagnetic $Cr^{III}Ni^{II}_6$. This apparent drawback become an useful tool for the distribution of local spins in the ground state of exchange-coupled magnetic systems.

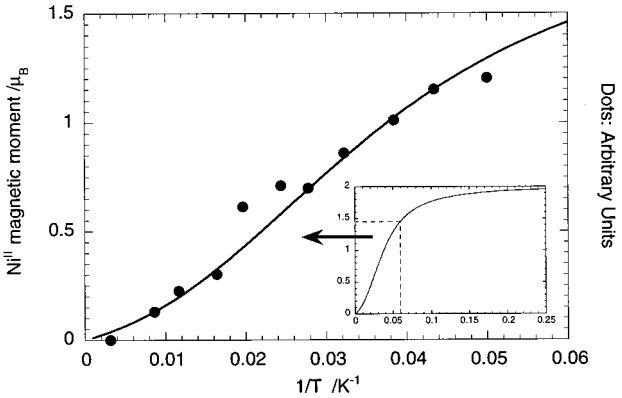

Figure 5. Experimental Ni^{II} L_3 edge maximum vs $1/T$ (●) compared to the theoretical Ni^{II}-specific magnetization curve (line) of $Cr^{III}Ni^{II}_6$ calculated for $H = 6$ T, $g = 2$, taking into account all of the spin states. Insert: theoretical Ni^{II} magnetization from high to low temperature.

IV. Variations of the Ni^{II} Magnetic Moment with Temperature in $Cr^{III}Ni^{II}_6$. We performed XMCD measurements at the Ni^{II} L_3 edge in a constant magnetic field (6 T) and at variable temperatures. In that configuration the spin states are split by the magnetic field and the population of the Zeeman states varies with the temperature. The experiment is expected to be sensitive to the different $|S,m_S\rangle$ states populations. To simplify the measurements, we only recorded the $\sigma_{\uparrow\uparrow}$ absorption spectra with an applied magnetic field parallel to the incident photon direction. We report in Figure 5 the variation of the L_3 edge with the reciprocal temperature.

The temperature-dependent magnetization curve was calculated using the spin Hamiltonian (2). The computed and experimental curves are compared in Figure 5. There is a good agreement between them. The insert in Figure 5 shows the computed magnetization down to very low temperature: 98% of the saturation magnetization is reached at 4 K and 65% at 20 K. The curve presents an inflection point at $T = 33$ K due to the contribution of the excited spin states. The behavior of the curve depends on the coupling strength: the curve becomes different from a Brillouin curve when the temperature is large compared to the J value. In the experimental temperature range, the Ni^{II} magnetic moment measured by XMCD follows the ascending part of the magnetization curve.

Conclusion

The current work presents one of the first XMCD measurements performed on molecular paramagnetic systems and allows the exploration of both the long-term interest and the present limitations of the technique.

The combination of ligand field multiplet calculations and of XMCD experiments performed at high magnetic field at the $L_{2,3}$ edges of each of the metallic components of multimetallic paramagnetic clusters makes possible to extend the conclusions already reached for magnetically ordered three-dimensional materials to paramagnetic species. It is now possible to compute the electronic structure of the different metallic ions in paramagnetic polymetallic systems, even in the case of a strong covalent bonding such as in Cr−CN where the π bonding is important, thanks to a proper use of the crystal field $10Dq$, of the Slater integrals, and of the electron charge transfer in the fit of the experimental data.

The orientation of the local magnetic moments in the applied magnetic field and therefore the direct evidence of the local exchange coupling (ferro- or antiferromagnetic) between the paramagnetic ions can be locally probed. For powders and badly crystallized compounds, XMCD is the unique technique able to give such a result.

A quantitative use of the technique is available for the description of the electronic structure of the metal from the edges and to get the M_L/M_S ratio from XMCD when there is no mixing between the L_2 and the L_3 edges.

We show also that XMCD can be used to follow the thermal variation of the element-specific magnetization to compare it with the macroscopic one. We found no proportionality between local and bulk magnetization, even if the difference between the two is very small, as theoretically expected.

Nevertheless, it appears that, when the temperature is not low enough, the contributions of the excited spin states are non-negligible. In our case (sample temperature = 20 K), the contributions of the excited spin states impede the observation of a simple Brillouin behavior. Very low temperatures are necessary to study the ground-state only. Dilution refrigerators such as the one developed by Cramer and co-workers[27] in the temperature range from 100 mK to 4 K will be very useful in the development of XMCD spectroscopy. In the future, the normalized difference between total and local magnetization at the Cr^{III} $L_{2,3}$ edges, which is theoretically large for an antiferromagnetic coupling (7% at $T = 0$ K), could be measured experimentally.

The availability of such cryostats combined with strong applied magnetic fields will render feasible in the near future the local (element-specific) observation of Zeeman effects and zero-field splitting in the ground state of paramagnetic polymetallic systems. This will be a unique way to extract the detailed information necessary to describe and to understand the origin of the ground-state anisotropy in polynuclear high-spin molecules, which is one of the promising developments in the bottom-up approach of the rapidly expanding field of nanosystems.

Acknowledgment. This work was supported by the French Education Ministry, the Centre National de la Recherche Scientifique, the Institut de Physique du Globe (IPGP contribution number) and the European Union (TMR Network ERBFMRXCT980181). We are grateful to Theo Thole whom we will miss. We thank Professor Steve Cramer for many helpful discussions and Doctor Jean-Paul Kappler for many instrumental developments on the beamlines.

JA983521J

(27) Bryant, C. Master Thesis, University of California, Davis, 1998.